Available online at www.sciencedirect.com
ScienceDirect
Journal of Sound and Vibration 308 (2007) 647–659
JOURNAL OF SOUND AND VIBRATION
www.elsevier.com/locate/jsvi

Active control of shock by gain scheduling

Dezhang Wang[a], Hidekazu Nishimura[b,*], Taro Shimogo[c]

[a]*Graduate School of Science and Technology, Chiba University, 1-33, Yayoi-cho, Inage-ku, Chiba, Japan*
[b]*Graduate School of System Design and Management, Keio University, 2-15-45, Mita, Minato-ku, Tokyo, Japan*
[c]*Department of Mechanical Engineering, Keio University, 3-14-1 Hiyoshi Kohoku-ku, Yokohama, Kanagawa, Japan*

Accepted 21 March 2007
The peer review of this article was organised by the Guest Editor
Available online 31 May 2007

Abstract

In this paper, we deal with the active control of shock caused by the collision between two objects so as to make the deformation of the shock-receiving object large and the deformation of the shock-giving object small. Since the shock-receiving object deforms from the elastic range to the plastic range, we formulate a linear parameter-varying system to cover all the ranges and apply gain-scheduled (GS) control. Also, we utilize a frequency weighting function with varying gain in order to improve the performance of shock control. The GS control system exerts a continuous input when the deformation of the shock-receiving object changes from the elastic range to the plastic range. It is verified experimentally that the designed GS controller is effective for the active control of shock and that the plastic deformation ratio between the two objects is increased.

1. Introduction

A shock-absorbing material is inserted into a collision surface in order to reduce the deformation and stress of two colliding objects. When an actuator is used to control the collision system of two objects instead of a passive material, active control of shock is hypothesized to be adaptable to the deformation of each object. The collision problem between two objects arises in, for example, a plastic forming machine, sports engineering, and the safety of vehicles. In the plastic forming machine, to form an object, it is necessary to utilize the maximum energy for forming the object and to suppress the stress caused in the hammer and the metal mold. Moreover, in the vehicle collision problem, injury to the passenger in the vehicle should be suppressed to as great an extent as possible even if the front part of the vehicle is extensively destroyed.

Shimogo et al. [1] have already proposed a collision model of two objects in which each object is a single-degree-of-freedom vibratory system and shown that the deformation ratio of one object to the other can be maximized through linear quadratic control on the basis of simulation results. Since the shock-receiving object deforms from the elastic range to the plastic range, we linearized the controlled object in the plastic

*Corresponding author. Tel.: +81 3 5427 1712; fax: +81 3 5418 6584.
E-mail address: h.nishimura@sdm.keio.ac.jp (H. Nishimura).
URL: http://www.sdm.keio.ac.jp (H. Nishimura).

0022-460X/$ - see front matter © 2007 Elsevier Ltd. All rights reserved.
doi:10.1016/j.jsv.2007.03.080

deformation range and designed two linear time-invariant (LTI) controllers for both ranges, so as to make the deformation of the shock-receiving object large and the deformation of the shock-giving object small. Linear quadratic integral (LQI) control and H_∞ control were used to design a controller and we demonstrated experimentally the active control of shock [2]. Furthermore, we applied final-state control to obtain a feedforward input that can bring the deformation of a shock-receiving object to a certain specific amount and discussed the relationships among contact stiffness, deformation time, deformation ratio and energy balance [3]. We examined the conditions necessary to realize a 'dynamical diode' that can transmit energy unilaterally from the shock-giving object to the shock-receiving object in Ref. [4].

Since separate H_∞ controllers were designed, respectively, in the elastic deformation range and the plastic deformation range, the control input was discontinuous when the controllers were switched [2]. In this paper, to design a controller that can cover both the elastic and plastic deformation ranges simultaneously, we derive a linear parameter-varying (LPV) system for the controlled object and apply a gain-scheduled (GS) control that can exert a smooth control input even if plastic deformation occurs. Thus, we examine a shock control system that can make the deformation of the shock-receiving object large and the deformation of the shock-giving object small, and compare its effectiveness with that of H_∞ control.

2. Dynamical model and experimental setup

2.1. Modeling

A dynamical model for a shock problem between two objects is shown in Fig. 1. The following are assumed in the model.

(I) Both objects A and B are single-degree-of-freedom systems.
(II) Viscous damping of the objects is disregarded.
(III) The elast-plastic deformation of object B has a bilinear characteristic and the deformation unilaterally increases.
(IV) The stiffness of the contact surface is constant.

In the shock-receiving object B, an element that deforms elast-plastically is inserted between the mass m_1 and the fixed wall. When the deformation x_1 exceeds x_a, the deformation mode of the element changes from the elastic deformation range to the plastic deformation range. The relationship between the spring constants k_0, k_1 and the Coulomb damper f_r is shown by the load–deflection curve in Fig. 2. The shock-giving object A collides with object B from the horizontal direction, and the deformation of object B is induced. Object A consists of the actuator m_2, the mass m_3, the elastic spring k_3, and the contact stiffness k_2.

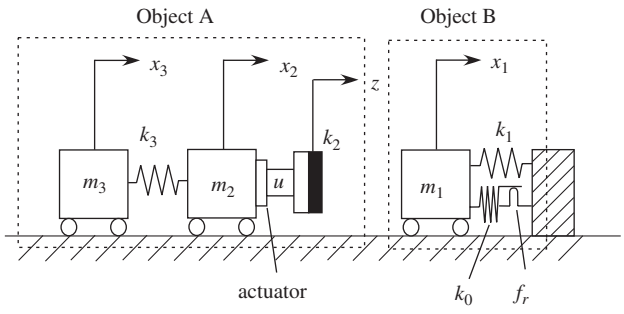

Fig. 1. Dynamical model.

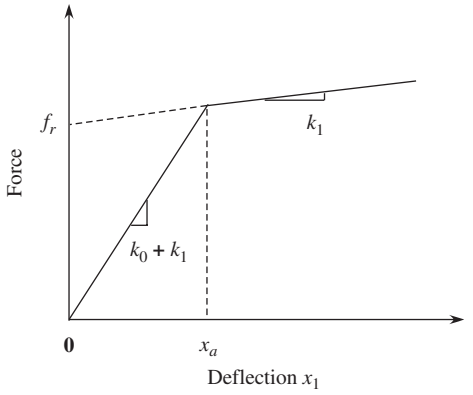

Fig. 2. Load–deflection characteristic of object B.

The equation of motion of the model is written as

$$\begin{aligned} m_1\ddot{x}_1 &= -k_1x_1 - P + k_2(z - x_1),\\ m_2\ddot{x}_2 &= -k_2(z - x_1) + k_3(x_3 - x_2),\\ m_3\ddot{x}_3 &= -k_3(x_3 - x_2), \end{aligned} \tag{1}$$

where x_1, x_2, and x_3 are the displacements of respective masses and z is the displacement of the moving part of the actuator. The P of the bilinear characteristic in Eq. (1) is described in the elastic deformation range and the plastic deformation range, respectively, as follows:

$$\begin{aligned} &x_1 \leqslant x_a : P = k_0x_1,\\ &x_1 > x_a : P = k_0x_a = f_r. \end{aligned}$$

If a speed servo-type actuator is used, the relationship between the input voltage u and the stroke velocity $\dot{y}_a = \dot{z} - \dot{x}_2$ is given as follows:

$$\dot{y}_a = au, \tag{2}$$

where a is a gain constant. Using $y_1 = x_1 - x_2$, $y_2 = x_2 - x_3$, $y_a = y_1 + z - x_1$, and the following state variable vector:

$$\mathbf{x} = [x_1,\ y_1,\ y_2,\ \dot{x}_1,\ \dot{y}_1,\ \dot{y}_2,\ z]^{\mathrm{T}}, \tag{3}$$

the state equations in the elastic range and in the plastic range can be, respectively, described as follows:

$x_1 \leqslant x_a$:

$$\dot{\mathbf{x}} = \mathbf{A}_l\mathbf{x} + \mathbf{B}u + \mathbf{E}_l, \quad \mathbf{y} = \mathbf{C}\mathbf{x} = [y_1\ y_a\ y_2]^{\mathrm{T}}, \tag{4}$$

$x_1 > x_a$:

$$\dot{\mathbf{x}} = \mathbf{A}_n\mathbf{x} + \mathbf{B}u + \mathbf{E}_n, \quad \mathbf{y} = \mathbf{C}\mathbf{x} = [y_1\ y_a\ y_2]^{\mathrm{T}}, \tag{5}$$

where

$$\mathbf{A}_* = \begin{bmatrix} \mathbf{0}_{3\times3} & \mathbf{I}_{3\times3} & \mathbf{0}_{3\times1} \\ \mathbf{A}_{1*} & \mathbf{A}_2 & \mathbf{A}_3 \end{bmatrix}, \quad * = l, n,$$

$$\mathbf{A}_{1*}=\begin{bmatrix} A_{11*} & 0 & 0 \\ A_{21*} & 0 & \dfrac{k_3}{m_2} \\ \dfrac{k_2}{m_2} & 0 & -\dfrac{k_3}{m_2}-\dfrac{k_3}{m_3} \\ 0 & 0 & 0 \end{bmatrix}, \quad \mathbf{A}_2=\begin{bmatrix} 0 & 0 & 0 \\ 0 & 0 & 0 \\ 0 & 0 & 0 \\ 1 & -1 & 0 \end{bmatrix},$$

$$\mathbf{A}_3=\begin{bmatrix} \dfrac{k_2}{m_1} & \dfrac{k_2}{m_1}+\dfrac{k_2}{m_2} & -\dfrac{k_2}{m_2} & 0 \end{bmatrix}^{\mathrm{T}}, \quad \begin{cases} A_{11l}=-\dfrac{k_0+k_1+k_2}{m_1} \\ A_{21l}=-\left(\dfrac{k_0+k_1+k_2}{m_1}+\dfrac{k_2}{m_2}\right), \end{cases}$$

$$\begin{cases} A_{11n}=-\dfrac{k_1+k_2}{m_1} \\ A_{21n}=-\left(\dfrac{k_1+k_2}{m_1}+\dfrac{k_2}{m_2}\right), \end{cases} \quad \mathbf{B}=[0\ 0\ 0\ 0\ 0\ 0\ a]^{\mathrm{T}},$$

$$\mathbf{E}_l=[0\ 0\ 0\ 0\ 0\ 0\ 0]^{\mathrm{T}}, \quad \mathbf{E}_n=[0\ 0\ 0\ -f_r/m_1\ -f_r/m_1\ 0\ 0]^{\mathrm{T}}.$$

2.2. Experimental setup

The experimental setup corresponding to Fig. 1 is shown in Fig. 3, and a schematic diagram is shown in Fig. 4. The parameters are shown in Table 1. The speed servo-type actuator is used to control the shock. The actuator has the following properties: the rated thrust is 300 N, the maximum thrust is 700 N, the peak-to-peak stroke is 35 mm, and the maximum speed is 2 m/s. The actuator stroke y_a can be detected with an incremental linear encoder built into the actuator and taken into a digital signal processor (DSP) through a counter board. A driving motor to give an initial speed $S_0=0.2$ m/s to object A is installed under a linear bearing that supports object A. The maximum thrust of this driving motor is 200 N and the rated speed is 0.5 m/s. Object A is pushed by the pushing parts of the driving motor whose speed follows a trapezium-like reference. After the driving motor decelerates, object A separates from the pushing parts and collides with object B by its inertia. Since there exists friction on the linear guide, the collision speed of object A should be compensated to be 0.23 m/s at the separation point, in order to ensure the collision speed of 0.2 m/s. Laser displacement sensors are used to detect the relative displacement between masses. Their measurement range is ±10 mm and their resolution is 2 μm. We confirm the actual colliding speed by differentiating of the signal of the laser sensor that detects the relative displacement between masses m_1 and m_2. The capacity of the strain gauge load sensor to detect the contact force f generated in the collision is 500 N. In the experiment, the signals of the laser displacement sensors and the load sensor are fed to the DSP through the analog/digital (A/D) converter and

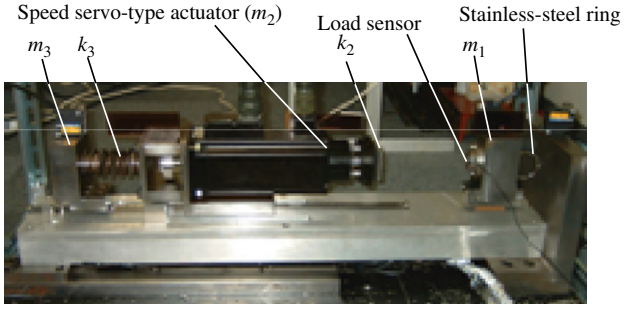

Fig. 3. Photograph of experimental setup.

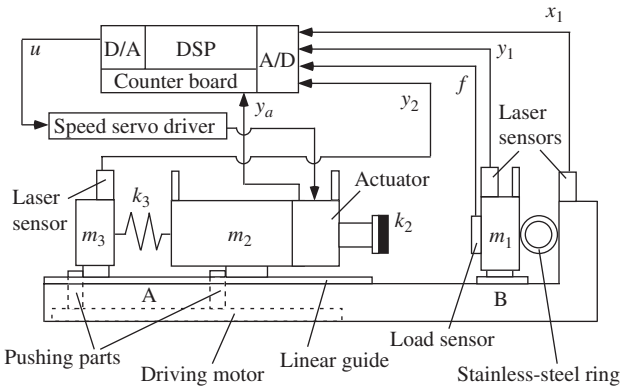

Fig. 4. Schematic diagram of experimental setup.

Table 1
Parameters of experimental setup

m_1	4.7 kg	$\overline{k}_2$	2.6×10^4 N/m
m_2	14.1 kg	k_3	7×10^4 N/m
m_3	4.6 kg	S_0	0.2 m/s

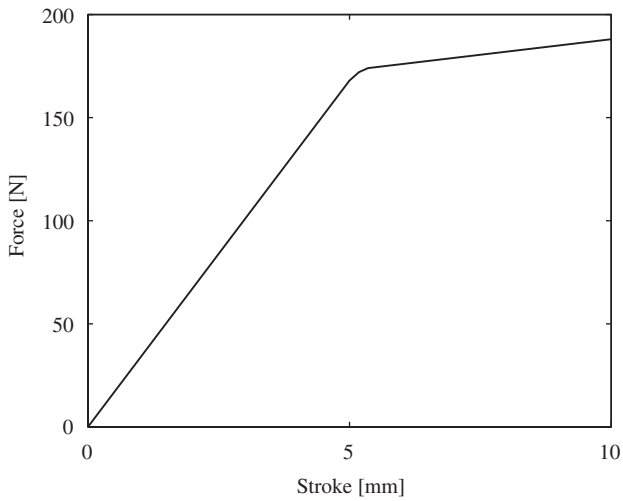

Fig. 5. Load–deflection curve of stainless-steel ring.

Table 2
Parameters of stainless-steel ring for controller design

k_0	2.8×10^4 N/m	f_r	140 N
k_1	1.8×10^3 N/m	x_a	5 mm

the control input is calculated. The control input is fed to the actuator driver through the digital/analog (D/A) converter and drives the speed servo-type actuator.

We use a stainless-steel ring as the specimen exhibiting elast-plastic deformation in object B. The outside diameter is 50 mm, the inside diameter is 47 mm and the width is 3 mm. From Ref. [5], the characteristic estimated is shown in Fig. 5 for the collision speed of 0.2 m/s. Table 2 shows the parameters of the stainless-steel ring.

3. Gain-scheduled controller design

3.1. Linear parameter-varying (LPV) model

The varying elements in the matrices $\mathbf{A}_l$ and $\mathbf{A}_n$ of Eqs. (4) and (5), respectively are in the following first row:

$$\mathbf{A}_l = \begin{bmatrix} 0 & \cdots \\ 0 & \cdots \\ 0 & \cdots \\ -\left(\frac{k_0}{m_1}+\frac{k_1}{m_1}+\frac{k_2}{m_1}\right) & \cdots \\ -\left(\frac{k_0}{m_1}+\frac{k_1}{m_1}+\frac{k_2}{m_1}+\frac{k_2}{m_2}\right) & \cdots \\ \frac{k_2}{m_2} & \cdots \\ 0 & \cdots \end{bmatrix}, \quad \mathbf{A}_n = \begin{bmatrix} 0 & \cdots \\ 0 & \cdots \\ 0 & \cdots \\ -\left(\frac{k_1}{m_1}+\frac{k_2}{m_1}\right) & \cdots \\ -\left(\frac{k_1}{m_1}+\frac{k_2}{m_1}+\frac{k_2}{m_2}\right) & \cdots \\ \frac{k_2}{m_2} & \cdots \\ 0 & \cdots \end{bmatrix}.$$

In $\mathbf{E}_l$ and $\mathbf{E}_n$, the fourth and fifth elements vary as follows:

$$\mathbf{E}_l = [0\ 0\ 0\ 0\ 0\ 0\ 0]^{\mathrm{T}}, \quad \mathbf{E}_n = \left[0\ 0\ 0\ -\frac{k_0}{m_1}x_a\ -\frac{k_0}{m_1}x_a\ 0\ 0\right]^{\mathrm{T}}$$

If we set the spring constant $k_0 = 2.8 \times 10^4\,\mathrm{N/m}$ as varying parameter p, the controlled object can be described as a LPV model by the following state equations:

$$\dot{\mathbf{x}} = \mathbf{A}(p)\mathbf{x} + \mathbf{E}(p) + \mathbf{B}u, \quad p \in [0\ 2.8 \times 10^4\,\mathrm{N/m}],$$

$$\mathbf{A}(p) = \begin{bmatrix} 0 & \cdots \\ 0 & \cdots \\ 0 & \cdots \\ -\left(\frac{p}{m_1}+\frac{k_1}{m_1}+\frac{k_2}{m_1}\right) & \cdots \\ -\left(\frac{p}{m_1}+\frac{k_1}{m_1}+\frac{k_2}{m_1}+\frac{k_2}{m_2}\right) & \cdots \\ \frac{k_2}{m_2} & \cdots \\ 0 & \cdots \end{bmatrix},$$

$$\mathbf{E}(p) = \left[0\ 0\ 0\ \left(\frac{p}{m_1}-\frac{k_0}{m_1}\right)x_a\ \left(\frac{p}{m_1}-\frac{k_0}{m_1}\right)x_a\ 0\ 0\right]^{\mathrm{T}}, \tag{6}$$

where the maximum value of the varying parameter p is $p_{\max} = k_0 = 2.8 \times 10^4\,\mathrm{N/m}$ in the elastic deformation range and its minimum value is $p_{\min} = 0$ in the plastic deformation range.

For the LPV model obtained by the above procedure, the gains of the frequency responses of the vertex model corresponding to the maximum and minimum values of the varying parameter are shown in Figs. 6 and 7, respectively. A GS controller may be designed for the LPV model so as to make as much as

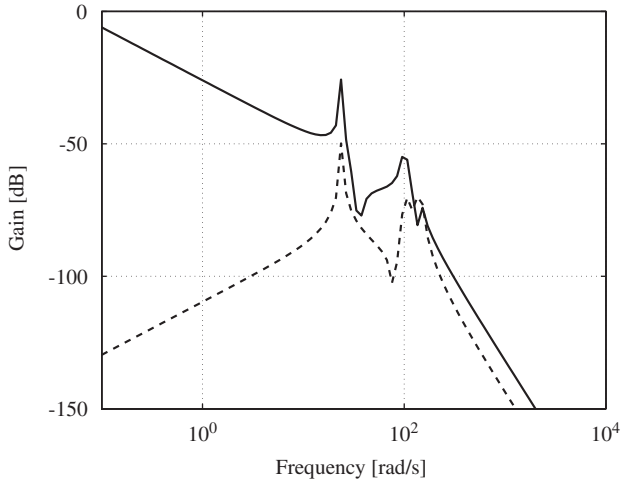

Fig. 6. Frequency response of controlled object in elastic range ($p = p_{\max}$).

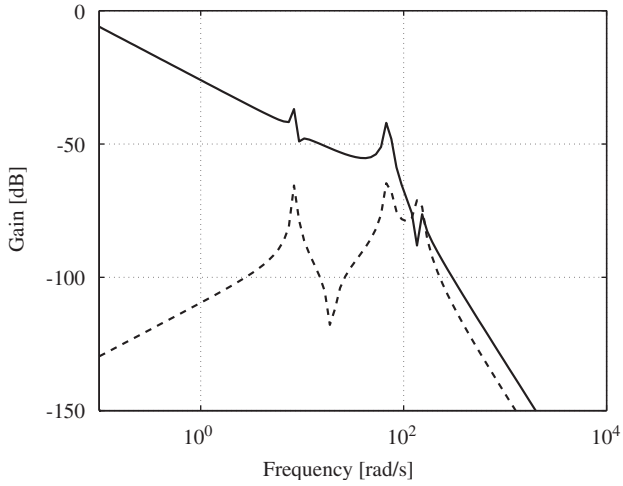

Fig. 7. Frequency response of controlled object in plastic range ($p = p_{\min}$).

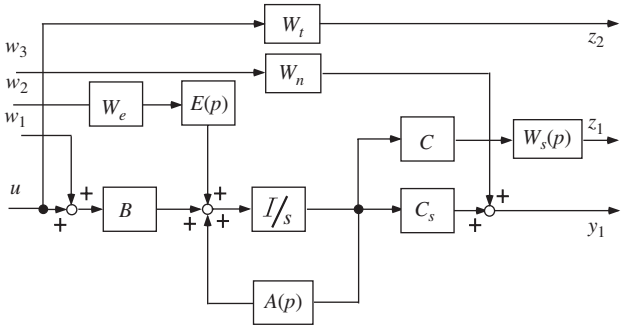

Fig. 8. Generalized plant.

possible the following plastic deformation ratio R_{pd}:

$$R_{pd} = \frac{x_{1\max} - x_a}{|y_2|_{\max}}. \tag{7}$$

3.2. GS control system using a weight depending on varying parameter

The GS control based on LMI [6] is applied to the obtained LPV model. The generalized plant used for the control system design is shown in Fig. 8. The feedback signal to the GS controller is the only the relative displacement y_1 between masses m_1 and m_2. In addition to y_1, relative displacement y_2 in object A and actuator stroke y_a are also evaluated. The matrixes $\mathbf{C}$ and $\mathbf{C}_s$ of Fig. 8 are

$$\mathbf{C} = \begin{bmatrix} 0 & 1 & 0 & 0 & 0 & 0 & 0 \\ -1 & 1 & 0 & 0 & 0 & 0 & 1 \\ 0 & 0 & 1 & 0 & 0 & 0 & 0 \end{bmatrix}, \quad \mathbf{C}_s = [0\ 1\ 0\ 0\ 0\ 0\ 0].$$

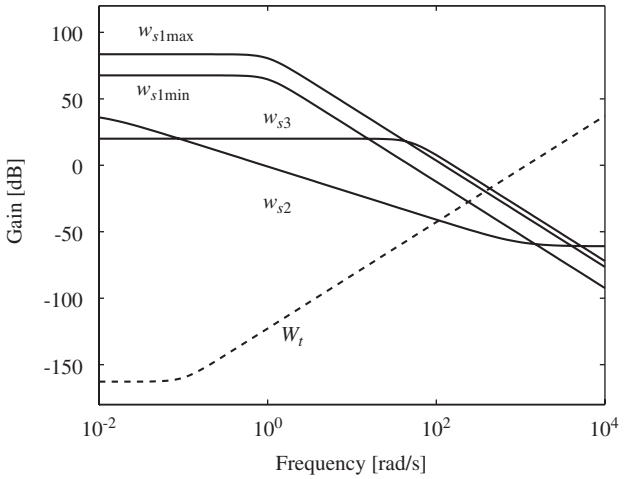

Fig. 9. Frequency weighting functions.

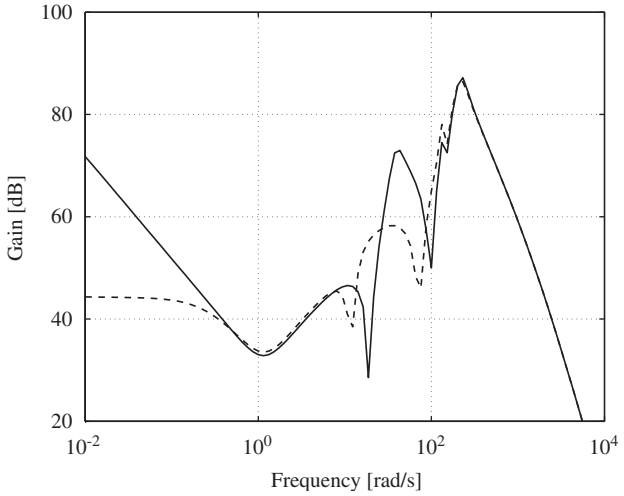

Fig. 10. Gain diagram of GS controllers.

Frequency weighting functions $\mathbf{W}_s(p) = \mathrm{diag}[w_{s1},\ w_{s2},\ w_{s3}]$ are used to evaluate the settling function from the disturbances w_1 and w_2 to the output z_1. As a measure of stability robustness for the modeling error, a frequency weighting function W_t is used.

For the range of varying parameter $p \in [0\ 2.8 \times 10^4\ \mathrm{N/m}]$, we could not design a GS controller that satisfies the following inequality:

$$\|G_{zw}\| < \gamma \tag{8}$$

and deforms the stainless-steel ring to the plastic deformation range. The reason is that the width of the varying parameter is too large. Thus, the minimum value of $p_{\min}$ is used as a design parameter. To make the value of $p_{\min}$ as small as possible, a constant weight W_e that is smaller than 1 is placed between disturbance w_2 and $\mathbf{E}(p)$ to lessen the variation of $\mathbf{E}(p)$ as shown in Fig. 8.

Since we have already verified that the plastic deformation ratio can be increased by reducing the control input after entering the plastic deformation range [2], we introduce a varying gain of the weighting function w_{s1} corresponding to the varying parameter p as follows:

$$w_{s1}(s) = \frac{1.5 \times 10^4 \times p/k_0}{s^2 + 1.41s + 1}. \tag{9}$$

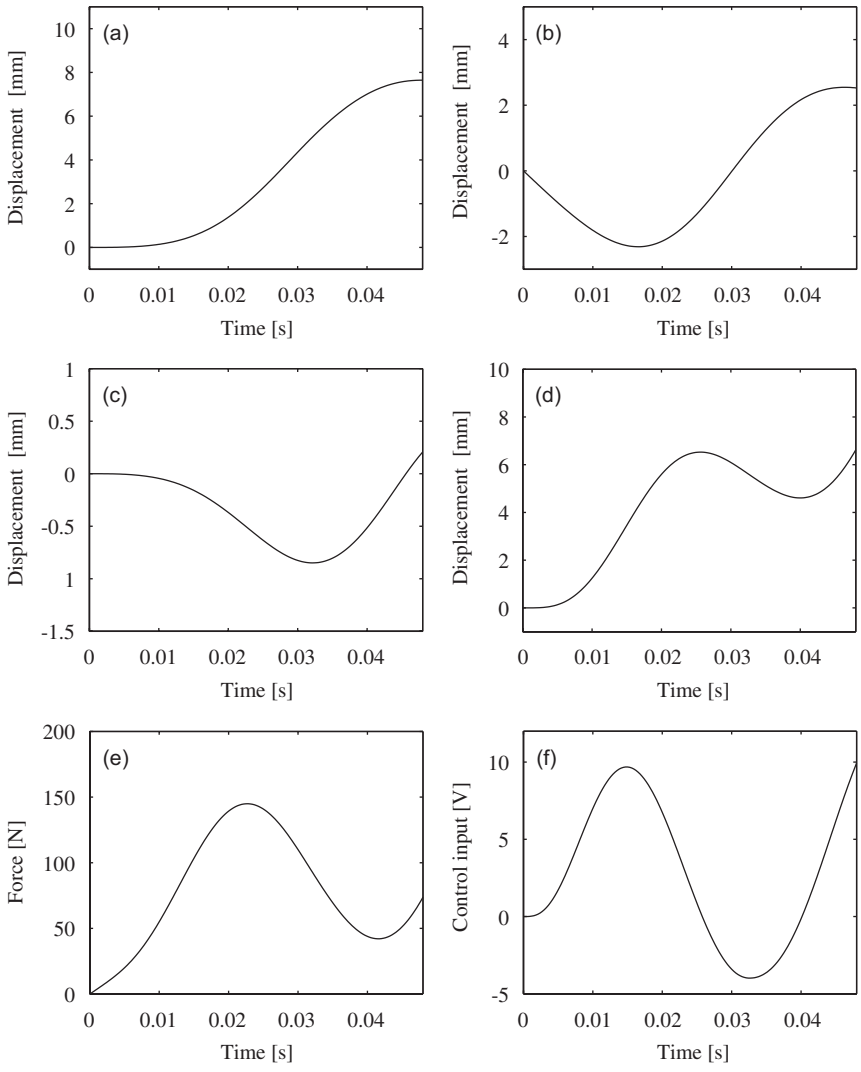

Fig. 11. Simulation results of time history response of GS controller (deformation ratio: 3.11).

To suppress the relative displacements y_1 and y_2 of object A, the gains of the weighting functions w_{s1} and w_{s3} are set large. Also, to loosen the restriction of actuator movement, the gain of the weighting function w_{s2} is set small.

Setting $p \in [4500\ 2.8 \times 10^4\,\mathrm{N/m}]$, $W_e = 0.8$ and the following frequency weighting functions, we obtained the GS controller that cannot only plastically deform the stainless-steel ring but also maximize the plastic deformation ratio R_{pd}. Functions w_{s2}, w_{s3}, and W_t are set as follows:

$$w_{s2}(s) = 90\frac{0.001s+1}{100s+1}, \quad w_{s3}(s) = \frac{2.5\times10^4}{s^2+70.7s+2.5\times10^3},$$

$$W_t(s) = 7.25\times10^{-4}\frac{s^2+0.141s+10^{-2}}{s^2+1.41\times10^4 s+10^8}. \tag{10}$$

The gain diagrams of frequency weighting functions are shown in Fig. 9. The frequency range of w_{s3} is set wider than those of the other functions in order to suppress the deformation y_2 of object A. To satisfy the necessary assumption of the H_∞ standard problem, observation noise w_3 is introduced, and $W_n = 0.1$.

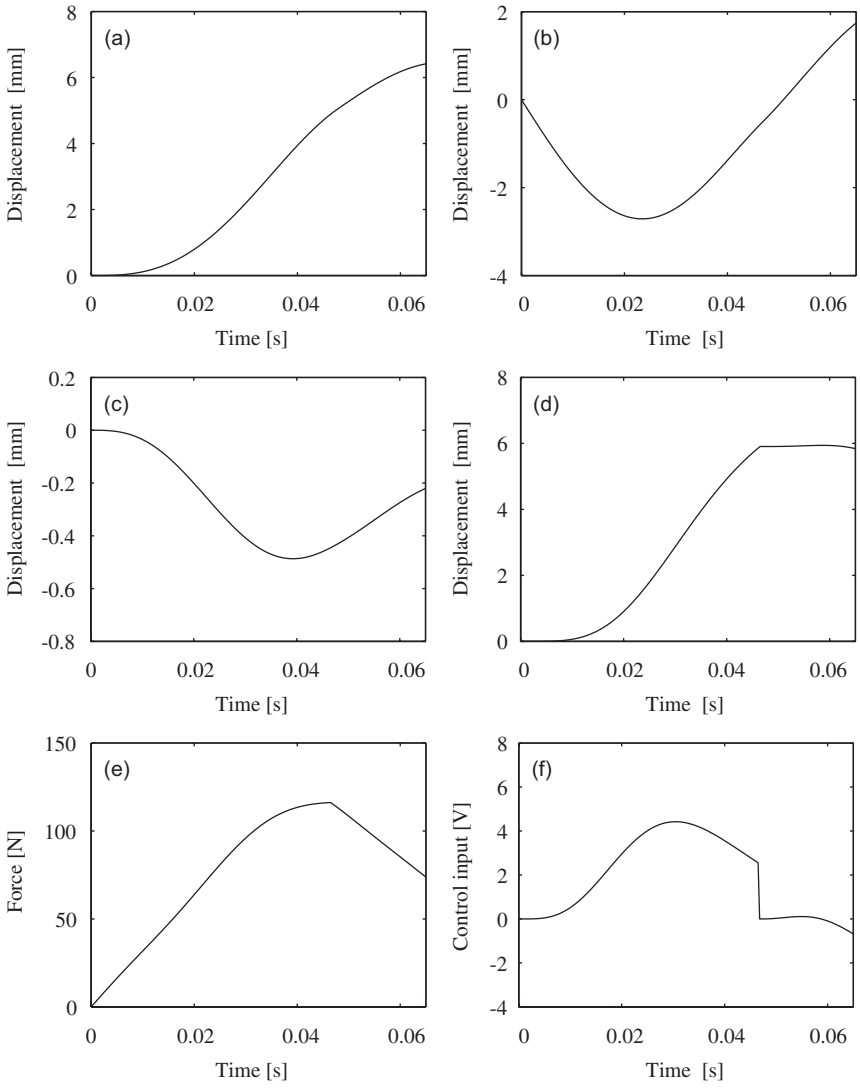

Fig. 12. Simulation results of time history responses of H_∞ controllers (deformation ratio: 2.98).

The gain diagrams of the vertex controllers are shown in Fig. 10. The gain for the elastic deformation range indicated by the solid line is larger than that for the plastic deformation range indicated by the broken line, in the whole frequency range except for the range from 20 to 27 rad/s. Since the designed vertex controllers are unstable, we have to arrange the control system in the experiment so as to keep the closed loop stable. It may be difficult to design stable controllers for both the elastic and plastic ranges that satisfy Eq. (8).

4. Simulation results

The simulation results of the designed GS controller are shown in Fig. 11. Fig. 11(a)–(f) show the deformation of object B, the relative displacement between m_1 and m_2, the deformation of object A, the actuator stroke, the

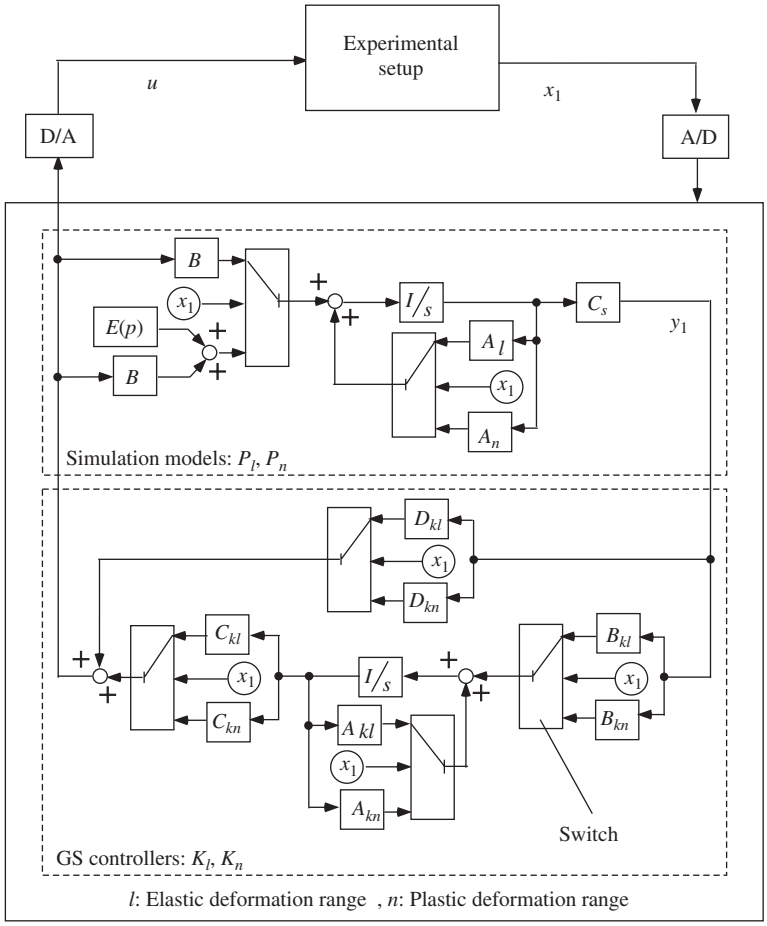

Fig. 13. Signal flow of GS controllers in DSP.

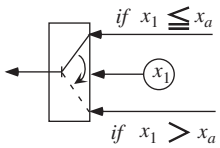

x_1: From A/D converter
x_a: Threshold

Fig. 14. Switching judgment.

contact force f, and the control input, respectively. Also, the simulation results of the H_∞ controller whose plastic deformation ratio R_{pd} is maximum are shown in Fig. 12. When the deformation of the stainless-steel ring shifts from the elastic deformation range to the plastic deformation range, the control input of the H_∞ control discontinuously changes as shown in Fig. 12(f) because of the controller's switching. Fig. 11(f) shows that the transition of the GS control input from the elastic deformation range to the plastic deformation range is smooth.

The maximum plastic deformation ratio R_{pd} of GS control is 3.11 and this value is more than that of the H_∞ control, 2.98. The GS controller can deform the stainless-steel ring in 48 ms. This deformation duration is smaller than that of the H_∞ controller, 62 ms. We have already concluded that as the deformation time increases, the plastic deformation ratio can also increase [3]. The GS control can enlarge the plastic deformation ratio even though the deformation time is shorter than that of the H_∞ control. If the deformation duration of the H_∞ controller is set to be 48 ms, the same as in Fig. 11, the R_{pd} of the H_∞ controller is reduced to 1.58.

5. Experiment

If the controller is unstable and noise is added into the feedback signal, the closed-loop system becomes unstable. Because the designed GS controller was unstable, we constructed, to solve this problem, a block

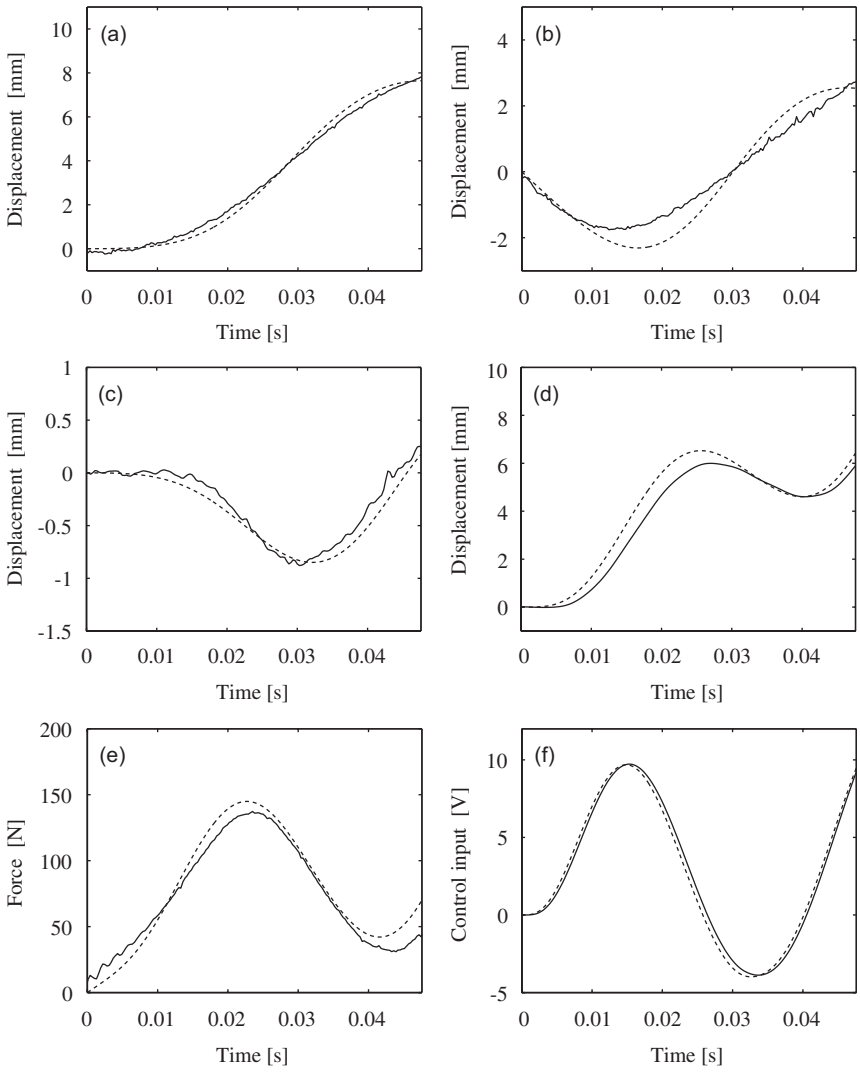

Fig. 15. Experimental results of time history response of GS controller (deformation ratio: 3.11).

where the control input is generated online in a sampling time of 0.3 ms from the closed-loop system using Simulink in the DSP as shown in Fig. 13. In Fig. 13, each switch switches from the upper side to the lower side when x_1 exceeds the threshold x_a as shown in Fig. 14. The subscript l denotes the elastic deformation range and the subscript n denotes the plastic deformation range. When the load sensor that is installed on the collision surface detects the collision of object A, the simulation of the closed-loop system starts and the control input u from the closed-loop system is fed into the actuator through the D/A converter.

The experimental results corresponding to the simulation results of Fig. 11 are shown in Fig. 15. It is seen that the experimental results are in good agreement with the simulation results.

6. Conclusion

We designed a control system for an actuator installed between two colliding objects where the shock-receiving object reached the plastic deformation range. A LPV system based on the deformation range was derived, and a control system that covers both elastic and plastic deformation ranges was obtained using a GS control method. A varying weighting function based on the deformation range is used in the controller design. It was shown that the controller was smoothly switched and made the deformation of the shock-receiving object large and that of the shock-giving object small. Thus, the obtained plastic deformation ratio is larger than that of H_∞ control. Also, the designed GS controller was unstable; thus, the block where the control input was generated online from the closed-loop system using Simulink was constructed in DSP. By carrying out experiments, it was verified that the experimental results are in good agreement with the simulation results.

Acknowledgements

This research was partially supported by Honda R&D Co., Ltd. This support is gratefully acknowledged.

References

[1] T. Shimogo, T. Kawashima, H. Sumi, Study on shock control, *Dynamics and Design Conference 2001 of the Japan Society of Mechanical Engineers*, 2001, 529.pdf (in Japanese).

[2] D.Z. Wang, H. Nishimura, T. Shimogo, Active control of shock (applications of LQI control and H_∞ control), *Transactions of the Japan Society of Mechanical Engineers, Series C* 71 (704) (2005) 1223–1230 (in Japanese).

[3] D.Z. Wang, H. Nishimura, T. Shimogo, Y. Amano, Active control of shock by using feedforward input, *Transactions of the Japan Society of Mechanical Engineers, Series C* 71 (710) (2005) 2912–2919 (in Japanese).

[4] H. Nishimura, D.Z. Wang, Y. Amano, T. Shimogo, Active control of shock, *ASME International Design Engineering Technical Conferences*, DETC2005-85623, 2005.

[5] M. Itoh, F. Yoshida, M. Ohmori, Combined effects of hydrostatic pressure and strain rate on the mechanical properties of a mild steel, *Materials Transactions JIM* 31-1 (1990) 46–50.

[6] P. Gahinet, A. Nemirovski, A.J. Laub, M. Chilali, *LMI Control Toolbox, For Use with MATLAB*, The MATHWORKS Inc., 1995.